

1 **Prior induction of cellular antiviral pathways limits frog virus 3 replication in two**
2 **permissive *Xenopus laevis* skin epithelial-like cell lines**

3
4 Maxwell P. Bui-Marinos ^a, Lauren A. Todd ^a, Marie-Claire D. Wasson ^a, Brandon E. E.
5 Morningstar ^a, and Barbara A. Katzenback ^a

6 ^a Department of Biology, University of Waterloo, Waterloo, Ontario, Canada, N2L 3G1

7

8

9

10

11

Correspondence:

12

Dr. Barbara A. Katzenback, PhD

13

Department of Biology

14

University of Waterloo

15

200 University Ave West

16

Waterloo, ON, N2L 3G1

17

Tel.: (519) 888-4567 × 30192

18

E-mail: barb.katzenback@uwaterloo.ca

19

20 **Abstract**

21 Frog virus 3 (FV3) causes mortality in a range of amphibian species. Despite the
22 importance of the skin epithelium as a first line of defence against FV3, the interaction between
23 amphibian skin epithelial cells and FV3 remains largely uncharacterized. Here, we used newly
24 established *Xenopus laevis* skin epithelial-like cell lines, Xela DS2 and Xela VS2, to study the
25 susceptibility and permissiveness of frog skin epithelial cells to FV3, and the innate immune
26 antiviral and proinflammatory gene regulatory responses of these cells to FV3. Both cell lines are
27 susceptible and permissive to FV3, yet do not exhibit appreciable transcript levels of scavenger
28 receptors recently demonstrated to be used by FV3 for cellular entry. Xela DS2 and Xela VS2
29 upregulate antiviral and proinflammatory cytokine transcripts in response to poly(I:C) but not to
30 FV3 or UV-inactivated FV3. Poly(I:C) pretreatment limited FV3 replication and FV3-induced
31 cytopathic effects in both cell lines. Thus, Xela DS2 and Xela VS2 can support FV3 propagation,
32 represent *in vitro* systems to investigate antiviral responses of frog skin epithelial cells, and are
33 novel tools for screening compounds that initiate effective antiviral programs to limit FV3
34 replication.

35

36 **Key words:** ranavirus, skin epithelial cells, innate immunity, poly(I:C), type I interferon,
37 amphibians

38 1. Introduction

39 *Frog virus 3* (FV3) is a large (105.9 kbp) double-stranded DNA virus and type species of
40 the *Ranavirus* genus, family *Iridoviridae*. In North America, ranaviruses are known to infect at
41 least 55 different amphibian species and have been implicated in mortality events in over 30 of
42 these species (Miller et al., 2011). Susceptibility to FV3 differs across amphibian species
43 (Hoverman et al., 2011) and within a species depending on the species' life stage, genotype
44 (Gantress et al., 2003), and environment (Brand et al., 2016). Susceptible amphibians exhibit
45 severe pathology such as skin lesions, swelling, and internal hemorrhage (Forzán et al., 2017;
46 Miller et al., 2007) that can result in up to 100% mortality in tadpoles (Haislip et al., 2011;
47 Hoverman et al., 2011) and post-metamorphs (Forzán et al., 2015), but appears to vary with
48 initial viral infection dose (Bienentreu et al., 2020). Relatively resistant amphibians develop mild
49 symptoms including lethargy, skin shedding and cutaneous erythema, but often recover in 2 – 3
50 weeks (Gantress et al., 2003) and instead may serve as asymptomatic reservoirs of FV3 (Robert
51 et al., 2007). Transmission of FV3 to naïve hosts can occur by water borne transmission or
52 consumption of infected carcass (Harp and Petranka, 2006; Robert et al., 2011) and necessitates
53 that FV3 evade a host epithelial barrier.

54 The African clawed frog (*Xenopus laevis*) was established as a model to study immune
55 responses to FV3 in the early 2000s (Gantress et al., 2003), and research using this model has led
56 to a basic understanding of the anuran anti-ranaviral immune response [reviewed in (Robert et
57 al., 2017)]. FV3 infection of adult *X. laevis* results in an increase in type I interferon (IFN) and
58 proinflammatory cytokine transcript levels in internal organs (De Jesús Andino et al., 2012;
59 Grayfer et al., 2014, 2015a), along with the recruitment of macrophages to the site of
60 intraperitoneal infection (De Jesús Andino et al., 2012). Type I IFN is critical for effective
61 antiviral defences against FV3, as pretreatment of the A6 *X. laevis* kidney epithelial cell line or
62 intraperitoneal injection of tadpoles with recombinant type I IFN prior to FV3 infection limited
63 viral replication (Grayfer et al., 2014). While these earlier studies demonstrated the importance
64 of amphibian type I IFN responses in antiviral defences, the use of intraperitoneal injection to
65 establish consistent FV3 infections in frog hosts largely precluded assessment of the antiviral
66 roles played by the skin barrier. However, as amphibian skin is in continuous interface with the
67 external environment, it represents an important innate immune barrier and first line of defence
68 against aquatic pathogens such as FV3 [reviewed in (Varga et al., 2019)]. More recent studies

69 have performed *in vivo* FV3 infections through water bath exposure, which more closely
70 approximates natural routes of FV3 transmission. These investigations have uncovered key roles
71 for type I and type III IFN responses in the skin of FV3-challenged *X. laevis* adults and tadpoles,
72 respectively (Wendel et al., 2017; Wendel et al., 2018), including the short-term protective
73 effects of subcutaneous administration of type I IFN or type III IFN, albeit to a lesser extent, in
74 highly susceptible *X. laevis* tadpoles against FV3 infection (Wendel et al., 2017).

75 While the above studies provide evidence that frog skin tissue contributes to antiviral
76 defence against FV3, the precise roles of each cell type within the skin have yet to be
77 determined. Skin tissue is complex and is comprised of many cell types, including epithelial and
78 fibroblast cells. Upon infection, additional cell types (i.e. macrophages and granulocytes) are
79 also recruited to the site of infection (Grayfer et al., 2015b). Macrophages appear to mediate
80 antiviral responses in relatively FV3-resistant hosts (Grayfer and Robert, 2014, 2015), but the
81 functions of other cell types in the anti-FV3 response require further investigation. The study of
82 whole skin tissue gives us meaningful information regarding how cells function synergistically to
83 respond to FV3, however, the complex cellular composition of skin tissue hinders our ability to
84 elucidate the individual contribution of each cell type to antiviral defences. Skin epithelial cells
85 are in constant direct contact with potential sources of FV3, yet the individual contribution of
86 skin epithelial cells to anti-FV3 defences remains largely uncharacterized.

87 To better investigate the initial interaction between frog epithelial cells and FV3, we
88 previously developed and characterized two skin epithelial-like cell lines from the dorsal and
89 ventral skin tissues of *X. laevis*, named Xela DS2 and Xela VS2, respectively (Bui-Marinos et
90 al., 2020). We have previously demonstrated that these cells can respond to poly(I:C), a synthetic
91 analogue of viral double-stranded RNA and potent inducer of type I IFN responses, through the
92 upregulation of antiviral and proinflammatory cytokine transcripts. In this study, we sought to
93 (1) evaluate whether Xela DS2 and Xela VS2 are susceptible and permissive to FV3, (2)
94 determine whether these cell lines initiate gene regulatory antiviral and proinflammatory
95 responses to FV3, and (3) uncover whether prior establishment of antiviral programs in these cell
96 lines would confer protection against FV3-associated cellular cytopathicity and limit viral
97 replication.

98 2. Methods

99 2.1. Xela DS2 and Xela VS2 cell lines and media

100 The generation, characterization and maintenance of the *X. laevis* dorsal (Xela DS2) and
101 ventral (Xela VS2) skin epithelial-like cell lines have been previously described by our research
102 group (Bui-Marinos et al., 2020). Briefly, Xela cell lines were sub-cultured every 3 – 4 days at a
103 1:4 split and cultured at 26 °C in plug-seal tissue culture treated flasks (BioLite; Thermo Fisher
104 Scientific) containing amphibian-adjusted Leibovitz's L-15 (AL-15; Wisent Inc.) medium
105 supplemented with 15% fetal bovine serum (FBS; VWR), herein referred to as Xela complete
106 media. Adherent cells were detached using 0.175% trypsin, 1.55 mM EDTA solution that was
107 prepared by diluting seven parts of 0.25% trypsin, 2.21 mM EDTA solution (Wisent Inc.) with
108 three parts of sterile ultrapure water. Amphibian phosphate-buffered saline (APBS) was similarly
109 prepared by diluting seven parts of sterile PBS with three parts of sterile ultrapure water. For all
110 experiments, seeding densities were adjusted to account for the plating efficiencies (79% for
111 Xela DS2 and 83% for Xela VS2). Since viral binding and infection efficiency is hindered at
112 high FBS concentrations (Petricevich et al., 2001), experiments involving FV3 infection of Xela
113 cell lines were performed using AL-15 supplemented with 2% FBS, herein referred to as Xela
114 low serum media.

115 2.2. *Epithelioma Papulosum Cyprini* (EPC) cells

116 EPC cells were kindly provided by Dr. Niels C. Bols (University of Waterloo, Ontario,
117 Canada) and were maintained at 26 °C in plug-seal tissue culture treated flasks containing
118 Leibovitz L-15 supplemented with 10% FBS, herein referred to as EPC complete media. EPC
119 cells were sub-cultured (1:4) every 5-7 days by washing with PBS and treatment with 0.25%
120 trypsin, 2.21 mM EDTA (Wisent Inc.) to detach adhered cells. Cells were collected by
121 centrifugation at $300 \times g$ for 10 min and resuspended in fresh EPC complete media. EPC cells
122 demonstrated 100% plating efficiency when enumerated the day after seeding. Although it is
123 known that current EPC cell lineages are contaminated with fathead minnow cells, they are still
124 deemed worth retaining as a cell line for the study of aquatic viruses (Winton et al., 2010). EPC
125 cells were selected for our experiments since they have been widely used to propagate and study
126 FV3 [e.g. (Ariel et al., 2009; Pham et al., 2015)]. For methods involving FV3 and EPC cells,

127 Leibovitz's L-15 supplemented with 2% FBS was used and will be referred to as EPC low serum
128 media.

129 **2.3. Propagation of FV3 in EPC cells**

130 FV3 (Granoff strain, ATCC VR-567) was a kind gift from Dr. Niels C. Bols (University
131 of Waterloo, Ontario, Canada). FV3 was propagated on EPC monolayers by adding 1 mL of
132 stock FV3 to 9 mL of EPC low serum media, and the entire volume was incubated on a
133 monolayer of EPC cells for 7 days at 26 °C. Seven days post-infection (dpi), virus-containing
134 media from the flask of infected EPC cells was collected, underwent three freeze-thaw cycles at
135 -80 °C, and was centrifuged at 1,000 × g for 10 min, filtered through a 0.22 µm PES filter
136 (FroggaBio), and aliquoted into sterile 1.5 mL microfuge tubes for storage at -80 °C.

137 **2.4. Determination of FV3 viral titres**

138 The tissue culture infectious dose wherein 50% of cells are infected (TCID₅₀/mL) values
139 were determined for viral stocks and experimental samples using the Kärber method (Kärber,
140 1931), further modified by Pham and colleagues (Pham et al., 2011). Briefly, EPC cells were
141 seeded in a 96-well tissue culture treated microwell plate (Thermo Fisher Scientific) at a final
142 cell density of 100,000 cells/well in 0.1 mL EPC complete media and allowed to adhere
143 overnight at 26 °C. The next day, the media was removed and 0.2 mL of a ten-fold dilution series
144 of the sample to be tested (prepared in EPC low serum media) was applied to EPC monolayers.
145 FV3-infected EPC cells were incubated for 10 d (determination of TCID₅₀/mL values for viral
146 stocks) or 7 d (determination of TCID₅₀/mL values for experimental samples) at 26 °C prior to
147 scoring for cytopathic effects (CPE). TCID₅₀/mL values were multiplied by a factor of 0.7 to
148 determine the approximate FV3 plaque forming unit (PFU)/mL values for multiplicity of
149 infection (MOI) calculations (Knudson and Tinsley, 1974).

150 **2.5. Resazurin and CFDA-AM assays**

151 Cellular metabolic activity and membrane integrity were evaluated using a combined
152 resazurin/5-carboxyfluorescein diacetate acetoxymethyl ester (CFDA-AM) assay (Dayeh et al.,
153 2004). To assess the viability of both adherent and suspension cells present in a well, stock
154 concentrations of resazurin (44 mM in APBS; Acros Organics) and CFDA-AM (800 µM in
155 DMSO; Invitrogen) were diluted in APBS to working concentrations of 4,400 µM and 40 µM,

156 respectively, before direct addition to the wells in a 1:10 ratio (final concentration of 440 μ M
157 resazurin and 4 μ M CFDA-AM). Direct addition of resazurin and CFDA-AM to the culture
158 media in each well permits viability assessment of both adherent and suspension cell
159 populations. Plates were protected from light and allowed to incubate for 1 h at 26 °C.
160 Fluorescence intensity was then measured for resazurin (535 nm/590 nm) and CFDA-AM (484
161 nm/530 nm) using a Cytation 5 multi-mode imaging plate reader (BioTek). In all cases, wells
162 containing resazurin/CFDA-AM solution but without cells were included as a background
163 control and their fluorescent values were subtracted from the values obtained from experimental
164 samples.

165 **2.6. Assessment of Xela DS2 and Xela VS2 susceptibility and permissibility to FV3**

166 To assess the susceptibility of Xela DS2 (passages 63 – 66) and Xela VS2 (passages 68 –
167 72) to FV3, cells were seeded in a 48-well tissue culture treated plate (BioLite) at a final cell
168 density of 50,000 cells/well in 0.3 mL Xela complete media and allowed to adhere overnight at
169 26 °C. The next day, media was removed, and cells were treated in triplicate with 0.25 mL of
170 Xela low serum media alone (mock-infected control) or containing FV3 at MOIs of 0.0002,
171 0.002, 0.02, 0.2, 2 or 20. After 2 h of virus absorption at 26 °C, media was removed, and wells
172 were washed three times with 300 μ L of APBS prior to the addition of 500 μ L of Xela low serum
173 media. Plates were sealed with parafilm and incubated at 26 °C for the duration of the
174 experiment. Total (adherent and suspension) cell viability was measured using the
175 resazurin/CFDA-AM assay (Section 2.5) after 0, 1, 3, 5, 7, 10, and 14 dpi. Four independent
176 trials were conducted ($n = 4$).

177 To assess the permissibility of Xela DS2 (passages 129 – 139) and Xela VS2 (passages
178 134 – 139) to FV3 replication, 250,000 cells/well were seeded in a 12-well plate (Thermo Fisher
179 Scientific) in 0.75 mL Xela complete media and allowed to adhere overnight at 26 °C. The next
180 day, media was removed from the wells and cells were treated with 0.5 mL of Xela low serum
181 media alone (mock-infected control) or containing FV3 at a MOI of 0.002, 0.02, 0.2, 2 or 20.
182 After 2 h of virus absorption at 26 °C, media was removed and wells were washed three times
183 with 0.5 mL of APBS, prior to the addition of 2.5 mL of fresh Xela low serum media to all wells.
184 Plates were sealed with parafilm and incubated at 26 °C. Phase contrast digital images and cell
185 culture media were collected on 0 (30 min post-wash), 1, 3, 5, and 7 dpi for all treatments. Phase
186 contrast digital images were captured using a Leica DMi1 microscope fitted with a MC170 color

187 camera and LAS X 4.8 software. Collected media was centrifuged at $500 \times g$ for 5 min, and
188 supernatants were transferred to sterile 1.5 mL microfuge tubes prior to storage at $-80\text{ }^{\circ}\text{C}$.
189 $\text{TCID}_{50}/\text{mL}$ values were determined as described in Section 2.4. This experiment was conducted
190 four independent times ($n = 4$).

191 **2.7. Detection of scavenger receptor transcripts**

192 Total RNA was isolated from 3×10^6 Xela DS2 (passages 28, 29 and 31) and Xela VS2
193 (passages 42, 46 and 48) using TRI reagent (Invitrogen) according to the manufacturer's
194 instructions with the following modifications: ground tissue samples were further homogenized
195 using a 1 mL syringe fitted with a 25-gauge needle and RNA pellets were washed with 1 mL of
196 75% ethanol (twice for cell lines and five times for tissues). RNA was quantified using a
197 NanoDrop 2000 spectrophotometer, and RNA quality was examined by electrophoresing $1\text{ }\mu\text{g}$ of
198 RNA on a 1% agarose gel containing 1% bleach (Aranda et al., 2012) and $1 \times$ RedSafe nucleic
199 acid staining solution (FroggaBio) in $1 \times$ TAE buffer at 100 V for 35 min. RNA was stored at
200 $-80\text{ }^{\circ}\text{C}$ until use.

201 RNA ($1\text{ }\mu\text{g}$) was treated with 0.5 U of DNase I (Thermo Fisher Scientific), DNase I was
202 heat-inactivated, and RNA was reverse-transcribed into cDNA using the $5 \times$ All-In-One RT
203 Master Mix (Bio Basic) according to the manufacturer's specifications ($25\text{ }^{\circ}\text{C}$ for 10 min, $42\text{ }^{\circ}\text{C}$
204 for 50 min and $85\text{ }^{\circ}\text{C}$ for 5 min). Genomic DNA contamination was excluded by employing a no
205 reverse-transcriptase (-RT) control. Synthesized cDNA was stored at $-20\text{ }^{\circ}\text{C}$ until use.
206 Subsequent PCR reactions were set up with the GeneDireX kit [$1 \times$ reaction buffer with 2 mM
207 MgCl_2 , 200 μM dNTPs, 200 nM (each) forward and reverse primers (Supplementary Table 1),
208 0.625 U *Taq* polymerase and 4 μL of 1:8 diluted cDNA]. Thermocycling conditions were as
209 follows: $95\text{ }^{\circ}\text{C}$ for 5 min, followed by 26 (*actb*) or 35 (scavenger receptors) cycles of $95\text{ }^{\circ}\text{C}$ for
210 30 sec, $55\text{ }^{\circ}\text{C}$ (*actb*) or $52\text{-}54\text{ }^{\circ}\text{C}$ (scavenger receptors) for 30 s and $72\text{ }^{\circ}\text{C}$ for 30 s, and a final
211 extension at $72\text{ }^{\circ}\text{C}$ for 10 min. One-third of the PCR volume was visualized on a 1% agarose gel
212 run in $1 \times$ TAE and imaged using a ChemiDoc imager (Bio-Rad). We validated each amplicon
213 by direct sequencing at The Centre for Applied Genomics (The Hospital for Sick Children) and
214 confirmed amplicon identity by BLASTn analysis (Altschul et al., 1990).

215 **2.8. UV inactivation of FV3**

216 FV3 aliquots were thawed and gently vortexed prior to exposure to 150 mJ UV energy
217 using a UV Crosslinker (BioRad), a dose which has been previously used to effectively
218 inactivate FV3 (Chinchar et al., 2003). FV3 inactivation was confirmed by measuring levels of
219 the viral *mcp* transcript (Supplementary Methods Section 5) and assessment of viral titres
220 (Section 2.4). UV-irradiated FV3 aliquots were stored at -80°C until use.

221 **2.9. Challenge of Xela DS2 and Xela VS2 with FV3**

222 Xela DS2 (passages 120 – 130) and Xela VS2 (passages 125 – 135) ($n = 4$ independent
223 trials) were seeded in a 6-well plate (Eppendorf) at a cell density of 625,000 cells/well in 1 mL
224 of Xela complete media and allowed to adhere overnight at 26°C . The next day, the media was
225 removed, and cells were treated with 0.5 mL of Xela low serum media alone (mock-infected
226 control), UV-inactivated FV3 (MOI 2), or FV3 (MOI 2). After 2 h incubation at 26°C , the media
227 was removed, wells were washed three times with 0.5 mL of APBS, and 2 mL of fresh Xela low
228 serum media was added to each well. To one of the monolayers previously incubated for 2 h with
229 Xela low serum media alone, Xela low serum media containing $1\ \mu\text{g/mL}$ poly(I:C) was added
230 (positive control). Phase-contrast images were taken of all treatments at 0, 6, 24, 48, and 72 h
231 post-treatment (commenced following the addition of fresh Xela low serum media) using a Leica
232 DMi1 microscope fitted with a MC170 color camera and LAS X 4.8 software to assess cell
233 morphology. At each time point, media was collected and centrifuged at $500 \times g$ for 5 min.
234 Cleared media was transferred to sterile 1.5 mL microfuge tubes and stored at -80°C for
235 determination of viral titres (see Section 2.4). Total RNA was isolated from combined adherent
236 and suspension cells using the EZ-10 Spin Column Total RNA Minipreps Super Kit (Bio Basic)
237 with the following modification: cells pelleted from culture media were suspended in 100 μL
238 lysis solution then mixed 1:1 with 70% ethanol and stored on ice. Meanwhile, remaining
239 adherent cells were washed once with 1 mL APBS, followed by the addition of 300 μL lysis
240 solution directly to wells for 1 min on ice, then mixed 1:1 with 70% ethanol. Lysates from the
241 suspension and adherent cells were combined and mixed by inversion prior to addition to spin
242 columns. Total RNA isolation, cDNA synthesis, and reverse transcriptase-quantitative
243 polymerase chain reaction (RT-qPCR) were performed as described in Section 2.10 and Section
244 2.11.

245 **2.10. Total RNA isolation and cDNA synthesis for antiviral gene expression assays**

246 Total RNA was isolated from Xela DS2, Xela VS2 and EPC cells using the EZ-10 Spin
247 Column Total RNA Minipreps Super Kit (Bio Basic) according to the manufacturer's
248 specifications with modifications to include an on-column DNase I digestion as described
249 previously by our group (Bui-Marinos et al., 2020). RNA quantity and purity were determined as
250 described in Section 2.7. RNA (500 ng) was reverse-transcribed into cDNA using the
251 SensiFAST cDNA Synthesis Kit (BioLine) according to the manufacturer's specifications for
252 synthesis of cDNA for use in RT-qPCR reactions. Synthesized cDNA was stored at -20 °C until
253 use.

254 **2.11. RT-qPCR**

255 Primer sequences, accession numbers, R^2 and primer efficiency values for *X. laevis tnf*,
256 *ill1b*, *cxcl8a*, *ikb*, *ifn*, *mx2*, *pkc*, *actb*, *cyp*, *ef1a*, *gapdh*, and *hgprt* targets used in this study have
257 been previously reported (Bui-Marinos et al., 2020). The type I IFN (*ifn*) primers targets a
258 conserved region of *ifn3*, *ifn4*, *ifn6* and *ifn7* from the expanded family of *X. laevis* type I IFNs
259 (Bui-Marinos et al., 2020). Gene stability measures (M-values) were determined for all
260 endogenous control candidates (*actb*, *cyp*, *ef1a*, *gapdh*, and *hgprt*; Supplementary Table 2) to
261 identify a suitable endogenous control, as described in (Bui-Marinos et al., 2020), using the
262 Applied Biosystems QuantStudio Analysis software, wherein a lower M-value infers stronger
263 gene stability across time and treatment. With M-values of 0.428 and 0.424 for Xela DS2 and
264 Xela VS2 samples, respectively, *actb* was selected as the endogenous reference gene for analysis
265 of relative transcript abundance.

266 For relative transcript abundance analysis, RT-qPCR reactions were prepared in duplicate
267 and consisted of 2.5 μ L of 500 nM sense and antisense primers, 5 μ L PowerUp SYBR green mix
268 (Thermo Fisher Scientific), and 2.5 μ L of diluted (1:20) cDNA template. Thermocycling
269 conditions were as follows: initial denaturation at 50 °C for 2 min, followed by 95 °C for 2 min
270 and 40 amplification cycles of denaturation at 95 °C for 1 s and extension at 60 °C for 30 s. A
271 melt curve step followed all runs to ensure only a single dissociation peak was present, with
272 initial denaturation at 95 °C for 1 s, then dissociation analysis at 60 °C for 20 s followed by 0.1
273 °C increments between 60 °C and 95 °C at 0.1 °C/s. Reactions were prepared in MicroAmp fast
274 optical 96-well reaction plates (Life Technologies), sealed with MicroAmp clear optical film

275 (Life Technologies) and run on a QuantStudio5 Real-Time PCR System (Thermo Fisher
276 Scientific).

277 **2.12. Effect of poly(I:C) treatment on Xela DS2 and Xela VS2 cell viability**

278 Xela DS2 (passages 33 – 35) and Xela VS2 (passages 41 – 43) cells were seeded in a 48-
279 well plate at a final cell density of 50,000 cells/well in 0.3 mL Xela complete media and allowed
280 to adhere overnight at 26 °C. The next day, media was removed, and cells were treated with 500
281 µL of Xela low serum media containing 0, 10, 50, 100, 1,000, or 10,000 ng/mL poly(I:C) and
282 incubated at 26 °C. Resazurin/CFDA-AM assays were performed as previously described
283 (Section 2.5) after 1, 2, 3, and 5 days post-treatment to measure total cell (adherent and
284 suspension) viability. Three independent trials were performed for each set of experiments ($n =$
285 3).

286 **2.13. Antiviral assays**

287 Xela DS2 (passages 135 – 140) and Xela VS2 (passages 138 – 143) cells were seeded in
288 a 48-well plate (Thermo Fisher Scientific) at a final cell density of 50,000 cells/well in 0.3 mL
289 Xela complete media and allowed to adhere overnight at 26 °C. The next day, media was
290 removed, and cells were pre-treated with 160 µL of Xela low serum media containing 0, 10, 50,
291 or 100 ng/mL poly(I:C) for 24 h at 26 °C, in sextuplicate. Following pretreatment, 90 µL of Xela
292 low serum media alone was added to three of the six replicates for all treatments (mock-
293 infected), and Xela low serum media containing FV3 (MOI 2) was added to the remaining
294 triplicate pre-treated wells. After incubation at 26 °C for 2 h, media was removed from all wells
295 which were then washed three times with 0.3 mL of APBS prior to the addition of 0.5 mL of
296 fresh Xela low serum media and subsequent incubation at 26 °C. After 0, 3, and 5 dpi, cell
297 culture media was collected, cleared by centrifugation at $500 \times g$ for 5 min, and transferred to
298 sterile 1.5 mL microfuge tubes prior to storage at -80 °C for future determination of TCID₅₀/mL
299 values (see Section 2.4). Afterwards, duplicate wells were treated with 200 µL of 440 µM
300 resazurin solution dissolved in APBS to determine adherent cell metabolic activity, and a single
301 well was treated with 200 µL Xela low serum media containing NucBlue Live reagent (Thermo
302 Fisher Scientific). Following 1 h of incubation in the dark, plates were read on a BioTek Cytation
303 5 multimode plate reader and imager using Gen5 software under the following conditions:
304 resazurin-treated wells were read with an excitation wavelength of 535 nm and emission

305 wavelength 590 nm, while the NucBlue Live-treated wells were fluorescently imaged with an
306 excitation wavelength of 377 nm and emission wavelength 477 nm to determine representative
307 cell counts for each respective treatment. Digital phase contrast images were captured in addition
308 to fluorescent imaging of NucBlue Live-treated cells. Four independent trials were conducted,
309 using cells from different passages for each trial ($n = 4$).

310 **2.14. Statistics**

311 Prior to all statistical analyses, datasets were tested for normality using the Shapiro-Wilks
312 test. Resazurin/CFDA-AM assay data for cellular viability after FV3 exposure (Section 2.6) and
313 poly(I:C) cytotoxicity (Section 2.12) data were analyzed using a two-way ANOVA test followed
314 by a Tukey's post-hoc test, or a Kruskal-Wallis test followed by Dunn's post-hoc test in cases
315 where data was not normally distributed (Supplementary Figure 1B). RT-qPCR (Section 2.11)
316 data were analyzed using a Kruskal-Wallis test followed by Dunn's post-hoc test. Data regarding
317 the effect of poly(I:C) pretreatment on FV3 replication based on cellular adherence and FV3
318 titres (Section 2.13) were analyzed using a two-way ANOVA test followed by a Tukey's post-
319 hoc test. All statistical analyses were performed using GraphPad Prism v8 software and groups
320 were considered statistically significant when $p < 0.05$.

321 **3. Results**

322 **3.1. Xela DS2 and Xela VS2 are susceptible and permissive to FV3**

323 The susceptibility of Xela DS2 and Xela VS2 to FV3 (MOI 0.002 – 20) was assessed
324 over 14 dpi using a combined resazurin/CFDA-AM assay to monitor changes in cell metabolic
325 activity and cell membrane integrity of the entire cell population. We observed FV3 MOI to have
326 a significant effect on the metabolic activity of Xela DS2 (Fig. 1A) and Xela VS2 (Fig. 1B)
327 (two-way ANOVA, $p < 0.0001$), along with a significant interaction between MOI and time
328 (two-way ANOVA, Xela DS2, $p = 0.0024$; Xela VS2, $p = 0.0002$). At a MOI of 20, a significant
329 decrease in cell metabolic activity was observed for Xela DS2 (Fig. 1A) and Xela VS2 (Fig. 1B)
330 as early as 3 dpi, and cell metabolic activity was virtually undetectable by 7 dpi. A significant
331 decrease in metabolic activity of Xela DS2 (Fig. 1A) and Xela VS2 (Fig. 1B) was also observed
332 as early as 5 dpi at a MOI of 2. Although not statistically significant, a decrease in metabolic
333 activity of Xela DS2 and Xela VS2 was also observed at 7 dpi at a MOI of 0.2 (Fig 1A, B,
334 respectively). A similar MOI-dependent decrease in cell membrane integrity was observed for

335 Xela DS2 (Fig. 1C) and Xela VS2 (Fig. 1D) (two-way ANOVA, $p < 0.0001$), as well a
336 significant interaction between MOI and time (two-way ANOVA, Xela DS2, $p = 0.0011$; Xela
337 VS2, $p = 0.0348$). No statistically significant differences were observed in relation to Xela DS2
338 or Xela VS2 metabolic activity or membrane integrity between mock-infected cells and FV3-
339 infected cells at a MOI of 0.02 or lower over 7 dpi (Fig. 1). A similar trend was observed at 14
340 dpi for both cell lines, although metabolic activity and membrane integrity were reduced and
341 somewhat variable by 14 dpi for both cell lines across all treatment groups (Fig. 1). FV3-infected
342 Xela DS2 and Xela VS2 monolayers (passages 129 – 139) exhibited dose- and time-dependent
343 CPE (Fig. 2A, B) that preceded the loss of cell viability (Fig. 1). CPE were characterized by cell
344 contraction and loss of adherence to the cell culture vessel, yielding floating cell clusters in the
345 culture media and culminating in complete destruction of the monolayer. While Xela DS2 (Fig.
346 2A) and Xela VS2 (Fig. 2B) exhibited CPE when infected with FV3 at higher MOI (0.02 – 20),
347 CPE was not observed in monolayers infected with FV3 at a MOI of 0.002. Similar dose- and
348 time-dependent changes in cell metabolic activity (Supplementary Figure 1B) and morphology
349 (Supplementary Figure 1A) were also observed in earlier passages (passage 20 – 55) of Xela
350 DS2 and Xela VS2 infected with FV3.

351 To assess whether Xela DS2 and Xela VS2 are permissive to FV3, monolayers were
352 mock-infected or infected with FV3 at MOIs of 0.002 – 20, and viral titres were measured over 7
353 dpi by determining TCID₅₀/mL values. Xela DS2 (Fig. 3A) and Xela VS2 (Fig. 3B) infected with
354 FV3 at a MOI of 0.02 or greater demonstrated marked increases in viral titres in a dose- and
355 time-dependent manner, with viral titre levels peaking at 5-7 dpi [maximal log₁₀(TCID₅₀/mL)
356 value of 6-7]. While Xela DS2 and Xela VS2 supported FV3 replication when infected at higher
357 MOIs (0.02 – 20), FV3 appeared unable to effectively replicate in Xela DS2 and Xela VS2 at a
358 MOI of 0.002 over the period examined (Fig. 3A, B). No viral particles were detected in culture
359 media collected from mock-infected (MOI 0) Xela DS2 or Xela VS2 at any time point (Fig. 3).
360 Similar time- and dose-dependent FV3 replication was observed in earlier passages (passage 30
361 – 50) of Xela DS2 and Xela VS2 as determined through viral titres (Supplementary Figure 1C)
362 and detection of viral transcripts (Supplementary Figure 2).

363 **3.2. Xela DS2 and VS2 do not express appreciable levels of class A scavenger receptors**
364 **thought to be used by FV3 during cellular entry**

365 Given that Xela DS2 and Xela VS2 are susceptible to FV3 infection, we sought to
366 examine the expression of class A scavenger receptors, a class of proteins that have been shown
367 to be used by FV3 during viral entry (Vo et al., 2019a). We examined the expression of
368 transcripts corresponding to class A scavenger receptors in Xela DS2 and Xela VS2. RT-PCR
369 analyses revealed a general lack of class A scavenger receptor (*srai/ii*, *scara3*, *scara4*, *scara5*,
370 *marco*) transcripts in Xela DS2 and Xela VS2, despite the detection of abundant levels in
371 reference tissues (Fig. 4). *scara3*, *scara4* and *scara5* transcripts were detected in control spleen
372 tissue as well as dorsal and ventral skin tissue, while *srai/ii* and *marco* transcripts were detected
373 in control spleen tissue but were undetected in dorsal and ventral skin tissue. Very low levels of
374 *scara3* and *scara5* transcripts were detected in two passages of Xela DS2 and Xela VS2 cells,
375 respectively.

376 **3.3. Xela DS2 and Xela VS2 do not upregulate antiviral or proinflammatory transcripts**
377 **when challenged with UV-inactivated FV3 or FV3**

378 We previously demonstrated that Xela DS2 and Xela VS2 upregulated key antiviral and
379 proinflammatory transcripts in response to poly(I:C), indicating that Xela DS2 and Xela VS2 are
380 capable of activating intrinsic antiviral pathways following recognition of a synthetic analogue of
381 viral double-stranded RNA (Bui-Marinos et al., 2020). To determine whether Xela DS2 and Xela
382 VS2 mount antiviral and proinflammatory responses to FV3 at the transcriptional level, Xela
383 DS2 and Xela VS2 were challenged with 1 µg/mL poly(I:C), UV-inactivated FV3 at a MOI of 2,
384 or FV3 at a MOI of 2, and mRNA levels of antiviral (*ifn*, *mx2*, and *pkr*), pro-inflammatory (*illb*,
385 *tnf*, and *cxcl8*) and *ikb* genes were measured using RT-qPCR. Similar to our previous study (Bui-
386 Marinos et al., 2020), poly(I:C) treatment of Xela DS2 and Xela VS2 resulted in significant
387 increases in *pkr* (Fig. 5E, F), *illb* (Fig. 6A, B), *tnf* (Fig. 6C, D), *cxcl8* (Fig. 6E, F) and *ikb* (Fig.
388 6G, H) transcript levels in comparison to the time-matched mock-treated cells (media alone) over
389 the 72 h examined, whereas no statistically significant changes in *ifn* (Fig. 5A, B) or *mx2* (Fig.
390 5C, D) transcript levels were observed at any time point. In contrast, challenge of Xela DS2 or
391 Xela VS2 with UV-inactivated FV3 or FV3 did not appear to induce the expression of the
392 antiviral (Fig. 5) or proinflammatory (Fig. 6) gene targets examined over the 72-h period, despite
393 observed changes in cell morphology that resulted in loss of cellular adherence to the tissue

394 culture vessel (Supplementary Figure 3). Although CPE were observed in Xela DS2 and Xela
395 VS2 challenged with UV-inactivated FV3 (MOI 2), transcripts for the FV3 *mcp* gene were
396 undetectable (Supplementary Figure 4A) and TCID₅₀/mL values did not increase over time
397 (Supplementary Fig. 4B, C), confirming that UV-inactivated FV3 could not undergo viral
398 replication. In contrast to these results, we detected *mcp* transcripts (Supplementary Figure 4A)
399 and observed increasing TCID₅₀/mL values in FV3-infected Xela DS2 and Xela VS2
400 (Supplementary Figure 4B, C).

401 **3.4. Evaluating poly(I:C) cytotoxicity in Xela DS2 and Xela VS2**

402 To evaluate potential cytotoxicity of poly(I:C), Xela DS2 and Xela VS2 were treated with
403 0 – 10,000 ng/mL of poly(I:C) and cell metabolic activity and membrane integrity were assessed
404 over 5 days post-treatment using a combined resazurin/CFDA-AM assay. The two highest doses
405 of poly(I:C), 1,000 ng/mL and 10,000 ng/mL, induced a significant loss in Xela DS2 cell
406 metabolic activity (Fig. 7A) and membrane integrity (Fig. 7C), and a significant loss in Xela VS2
407 cell metabolic activity (Fig. 7B) and membrane integrity (Fig. 7D) at virtually all time points
408 examined. No statistically significant differences in cell metabolic activity or cell membrane
409 integrity were observed in Xela DS2 or Xela VS2 across all days when cells were treated with 10,
410 50 or 100 ng/mL poly(I:C) compared to the non-treated, time-matched controls (Fig. 7). Due to
411 the decrease in Xela DS2 and Xela VS2 cell viability in the presence of high concentrations of
412 poly(I:C), poly(I:C) concentrations of 100 ng/mL or less were used in subsequent experiments.

413 **3.5. Poly(I:C) pretreatment confers partial protection against FV3-induced CPE in Xela** 414 **DS2 and Xela VS2**

415 To assess the potential effects of poly(I:C) pretreatment on susceptibility of Xela DS2
416 and Xela VS2 to FV3, cells were pre-treated with 0, 10, 50 or 100 ng/mL of poly(I:C) for 24 h
417 before mock-infection or FV3 infection (MOI 2). To quantify FV3-induced loss of cellular
418 adherence, adherent Xela DS2 (Fig. 8A, Supplementary Figure 5A) and Xela VS2 (Fig. 8B,
419 Supplementary Figure 5B) cell nuclei were enumerated and the numbers of adherent cells in each
420 of the FV3-infected groups were expressed as percentages relative to the number of adherent
421 cells in the corresponding pre-treated, mock-FV3 infected group. Two-way ANOVA analyses
422 indicated a significant effect of time ($p < 0.0001$) and poly(I:C) pretreatment concentration ($p <$
423 0.0001), accompanied with a significant interaction between these two factors ($p < 0.0001$), on

424 both Xela DS2 (Fig. 8A) and Xela VS2 (Fig. 8B) cell adherence. At 0 dpi and 3 dpi, no
425 statistically significant differences in adherent cell numbers were observed in FV3-infected Xela
426 DS2 (Fig. 8A) or Xela VS2 (Fig. 8B) across any of the poly(I:C) pre-treated groups. By 5 dpi,
427 we observed significant CPE characterized by a loss of cellular adherence in FV3-infected Xela
428 DS2 pre-treated with 0 or 10 ng/mL of poly(I:C) (Fig. 8A, Supplementary Fig. 5A). Meanwhile,
429 pretreatment of Xela DS2 with 50 or 100 ng/mL of poly(I:C) pretreatment appeared to
430 completely mitigate FV3-induced CPE as determined by enumerating adherent cell nuclei (Fig.
431 8A, Supplementary Figure 5A) and inspection of phase contrast images (Supplementary Figure
432 6A). In Xela VS2, poly(I:C) pretreatment was able to mitigate FV3-induced CPE in a dose-
433 dependent manner with the 50 and 100 ng/mL poly(I:C) pretreatments conferring partial and
434 complete mitigation of FV3-induced CPE, respectively (Fig. 8B, Supplementary Figure 5B,
435 Supplementary Figure 6B). Cellular adherence of Xela DS2 (Supplementary Figure 5A) or Xela
436 VS2 (Supplementary Figure 5B) was not affected in any of the poly(I:C)-treated mock-infected
437 groups over the course of the experiment.

438 Similar mitigation of FV3-induced CPE was observed in poly(I:C) pre-treated FV3-
439 infected Xela DS2 (Fig. 8C) and Xela VS2 (Fig. 8D) as assessed through a cell metabolic assay
440 as a proxy for cell viability. Two-way ANOVA analysis indicated that there was a significant
441 effect due to time ($p = 0.0004$ for Xela DS2, $p < 0.0001$ for Xela VS2) and poly(I:C)
442 pretreatment concentration ($p = 0.0159$ for Xela DS2, $p = 0.0002$ for Xela VS2), accompanied
443 with a significant interaction between these two factors ($p = 0.0308$ for Xela DS2, $p < 0.0001$ for
444 Xela VS2), on Xela DS2 (Fig. 8C) and Xela VS2 (Fig. 8D) cell metabolic activity. Pretreatment
445 of Xela DS2 with 50 or 100 ng/mL of poly(I:C), but not 10 ng/mL, was able to abrogate FV3-
446 induced CPE (Fig. 8C), while pretreatment of Xela VS2 with 50 or 100 ng/mL poly(I:C)
447 provided partial or complete abrogation of FV3-induced CPE, respectively (Fig. 8D).

448 **3.6. Poly(I:C) pretreatment limits FV3 replication in Xela DS2 and Xela VS2**

449 To determine whether poly(I:C) pretreatment limited FV3 replication, Xela DS2 or Xela
450 VS2 were pre-treated with low serum media alone [0 ng/mL poly(I:C)] or containing 100 ng/mL
451 poly(I:C) for 24 h prior to their infection with FV3. TCID₅₀/mL values were determined for
452 virus-containing cell culture media collected from 0, 3 and 5 dpi FV3-infected Xela DS2 or Xela
453 VS2 cells that had been pre-treated with either 0 ng/mL or 100 ng/mL of poly(I:C) (Fig. 9). Two-

454 way ANOVA analysis indicated a significant effect of time (Xela DS2, Xela VS2, $p < 0.0001$)
455 and poly(I:C) pretreatment (Xela DS2, $p < 0.0001$; Xela VS2, $p = 0.0106$), accompanied with a
456 significant interaction between these two factors (Xela DS2, $p < 0.0001$; Xela VS2, $p = 0.0063$),
457 on Xela DS2 and Xela VS2 TCID₅₀/mL values. Poly(I:C) pretreatment at 100 ng/mL limited
458 FV3 replication in both Xela DS2 (Fig. 9A) and Xela VS2 (Fig. 9B) compared to non-pretreated
459 cells that showed a time-dependent increase in TCID₅₀/mL values. Although cell culture media
460 from poly(I:C) pretreated Xela DS2 had higher TCID₅₀/mL values at 3 dpi compared to 0 dpi,
461 there was a significant reduction in TCID₅₀/mL values compared to the non-treated infected
462 control at 3 dpi. By 5 dpi, the TCID₅₀/mL values of cell culture media from poly(I:C) pretreated
463 Xela DS2 were significantly lower than the time-matched infected group, to the extent that these
464 values were not statistically different from either of the 0 dpi treatment groups (Fig. 9A). In
465 contrast, poly(I:C)-pretreated Xela VS2 did not appear to limit FV3 TCID₅₀/mL values to the
466 same extent, with a significant reduction in TCID₅₀/mL values only observed at 5 dpi in the cell
467 culture media of the poly(I:C) pre-treated group relative to the non-treated group (Fig. 9B).

468 4. Discussion

469 As amphibian skin epithelial cells are the first cellular line of defence against invading
470 pathogens, examining the initial response of these cells to FV3 is essential to furthering our
471 understanding of FV3 pathogenesis. Our previous research resulted in the successful expansion
472 of the *X. laevis* invitrome to include two novel skin-epithelial cell lines (Xela DS2 and Xela VS2)
473 that demonstrate the ability to initiate antiviral and proinflammatory gene regulatory responses
474 upon treatment with poly(I:C), a known inducer of type I IFNs (Bui-Marinos et al. 2020). In this
475 study, we utilized Xela DS2 and Xela VS2 as a novel platform to evaluate frog skin epithelial
476 cell permissibility to FV3, characterize frog skin epithelial cell antiviral and proinflammatory
477 gene regulatory responses to FV3 and UV-inactivated FV3, and demonstrate prior establishment
478 of antiviral programs in these cell lines confers protection against FV3 infection.

479 Xela DS2 and Xela VS2 skin epithelial-like cells appear equally permissive to FV3 and
480 exhibit cell rounding and detachment CPE similar to that observed in other FV3-permissive cell
481 lines (Chinchar et al., 2003; Pham et al., 2015). Xela DS2 and Xela VS2 produce relatively high
482 levels of infectious FV3 virions [$\log_{10}(\text{TCID}_{50}/\text{mL})$ of 6-7], albeit not to the same levels
483 observed in the EPC cell line [$\log_{10}(\text{TCID}_{50}/\text{mL})$ of 8-9] (Pham et al., 2015). However, Xela DS2

484 and Xela VS2 monolayers do not achieve the same cell density as EPC monolayers and the
485 apparent lower production of infective FV3 particles may be a result of fewer host cells to act as
486 viral factories. Interestingly, while Xela DS2 and Xela VS2 are permissive to FV3 at higher
487 MOIs (> 0.02), CPE and increases in TCID₅₀/mL values were not observed when these cell lines
488 were infected with FV3 at a MOI of 0.002 over the seven days examined, even though low levels
489 of viral particles were detected. It is possible this lack of viral replication at a low MOI is due to
490 ineffective binding of viral particles or some level of cell-intrinsic viral restriction in Xela DS2
491 and Xela VS2. Our findings support the use of Xela DS2 and Xela VS2 to propagate FV3 and for
492 use as *in vitro* models in which interactions between frog skin epithelial cells and FV3 can be
493 examined.

494 FV3 exists as enveloped and non-enveloped/naked virions and is known to enter host
495 cells through receptor-mediated endocytosis (enveloped virions) or fusion at the plasma
496 membrane followed by nucleocapsid injection into the cytoplasm (naked virions) (Braunwald et
497 al., 1985; Gendrault et al., 1981; Houts et al., 1974; Kelly, 1975). In contrast to previous studies
498 that demonstrated that FV3 uses class A scavenger receptors for cellular entry in tadpole cell
499 lines (American toad, wood frog, green frog, bullfrog) and adult *X. laevis* macrophages (Vo et al.,
500 2019a), Xela DS2 and Xela VS2 do not express appreciable levels of class A scavenger receptor
501 (*srai/ii*, *scara3*, *scara4*, *scara5*, and *marco*) transcripts despite being susceptible and permissive
502 to FV3. Although we did not examine Xela DS2 and Xela VS2 for the presence of class A
503 scavenger receptor proteins, our data suggests that either FV3 is utilizing different cell-surface
504 receptors for endocytosis-mediated entry, or that primarily naked FV3 virions are entering Xela
505 DS2 and Xela VS2. Given the broad cell and tissue tropism of FV3, it is likely that additional
506 host cell receptors are utilized by FV3 to gain entry to diverse cell types/tissues and warrants
507 further study.

508 As Xela DS2 and Xela VS2 are derived from *X. laevis* skin and are epithelial-like, these
509 cell lines serve as ideal *in vitro* systems to expand the arsenal of *X. laevis* resources at our
510 disposal to investigate frog skin epithelial antiviral defences against FV3. Although susceptible
511 to FV3, Xela DS2 and Xela VS2 failed to induce the expression of the key antiviral and
512 proinflammatory transcripts measured herein when infected with FV3 or UV-inactivated FV3.
513 Our observations agree with the current theory that FV3 encodes a capsid protein that is

514 responsible for the immediate immunoevasion of host antiviral pathways independent of viral
515 transcription (Robert et al., 2017; Rothenburg et al., 2011). However, our findings contrast with
516 observations of induction of innate antiviral pathways, such as type I IFN transcripts, in response
517 to FV3 infection of adult *X. laevis* skin tissue *in vivo* and adult *X. laevis* skin cells (mixed cell
518 type populations isolated from whole tissues) *in vitro* (Wendel et al., 2017; Wendel et al., 2018).
519 We propose that the interactions between skin epithelial cells and macrophages (or perhaps other
520 cell types) present in skin tissues may explain this discrepancy. In *X. laevis*, macrophages have
521 been identified as important mediators of FV3 infection (Grayfer and Robert, 2014) and distinct
522 differentiated macrophage subpopulations have been demonstrated to condition cell media with
523 type I IFNs that can be used to confer resistance to FV3 in the susceptible *X. laevis* kidney
524 epithelial A6 cell line (Yaparla et al., 2018). As macrophages have been found to reside in frog
525 skin (Fox and Whitear, 1990; Lehman, 1953), we hypothesize that initial FV3 replication in skin
526 epithelial cells and subsequent cell death leads to the release of viral material (e.g. apoptotic
527 bodies; viral RNA through cell necrosis) that is phagocytosed by resident and/or recruited
528 macrophages. Activation of antiviral programs in macrophages following the detection of
529 exogenous viral pathogen-associated molecular patterns (PAMPs) by endosomal pattern
530 recognition receptors may account for the detection of type I IFN transcripts observed in frog
531 skin tissues or in mixed cell type populations. Secretion of type I IFN by activated macrophages
532 would initiate antiviral programs in neighbouring skin cells, thus potentially conferring
533 protection to FV3 replication in skin tissues. Collectively, these observations highlight the
534 importance of studying the contributions of individual cell types and as well as cellular
535 interactions within complex skin tissue environments.

536 Simulation of Xela DS2 or Xela VS2 with higher concentrations of extracellular poly(I:C)
537 [10 µg/mL, (Bui-Marinos et al., 2020); 1 µg/mL, this study] results in a modest induction of
538 antiviral genes and a robust upregulation of proinflammatory cytokine genes, strongly supporting
539 that idea that frog skin epithelial cells are important cellular participants in mediating skin
540 antiviral defences, in addition to their role as a physical barrier. Aside from regulating antiviral
541 and proinflammatory genes, concentrations of poly(I:C) above a threshold (> 100 ng/mL) are
542 cytotoxic to Xela DS2 and Xela VS2. Similar poly(I:C)-induced cytotoxicity has been noted in
543 an *Anaxyrus americanus* tadpole cell line (Vo et al., 2019b), yet many other vertebrate cells do
544 not exhibit poly(I:C)-induced cytotoxicity at these concentrations [e.g. (Kumar et al., 2006;

545 Ritter et al., 2005)]. Our findings suggest that an increased sensitivity of frog skin epithelial cells
546 to viral nucleic acids may be advantageous for removal of infected cells to limit viral spread and,
547 together with the induction of effector proinflammatory cytokines and chemokines, is an
548 important antiviral defence mechanism of frog skin epithelial cells.

549 To ascertain frog skin epithelial cell immunocompetence in relation to functional viral
550 restriction to FV3, we prestimulated Xela DS2 and Xela VS2 with poly(I:C) concentrations
551 below the observed threshold for poly(I:C)-induced cytotoxicity (100 ng/mL or less) prior to
552 FV3 infection. Consistent with previous observations of reductions in FV3 replication following
553 pretreatment of *X. laevis* A6 cells with type I IFN (Grayfer et al., 2014), subcutaneous injection
554 of *X. laevis* tadpoles with type I IFN (Wendel et al., 2017), or pretreatment of rainbow trout
555 gonadal fibroblast cell lines with poly(I:C) (Lisser et al., 2017), pretreatment of Xela DS2 and
556 Xela VS2 with low concentrations of poly(I:C) mitigated FV3-induced CPE and limited FV3
557 replication. It is likely that these antiviral effects are the result of the induction of type I IFN-
558 mediated antiviral programs, as poly(I:C) is a well-known inducer of type I IFN and we have
559 shown that poly(I:C) induces the expression of antiviral and proinflammatory gene transcripts in
560 these cell lines [this study and (Bui-Marinos et al., 2020)]. Interestingly, the induction of
561 functional anti-FV3 restrictions and its protective effects appear stronger in Xela DS2 than Xela
562 VS2, as immune gene transcripts are generally induced earlier in response to poly(I:C) treatment
563 [this study and (Bui-Marinos et al., 2020)] and protection against FV3 replication is achieved at
564 lower poly(I:C) doses, and to a greater extent, in Xela DS2 compared to Xela VS2. Whether the
565 differential induction of poly(I:C) mediated anti-FV3 responses observed between Xela DS2 and
566 Xela VS2 are reflective of physiological differences between skin epithelial cells from the dorsal
567 and ventral skin, as well as the underlying mechanism(s) driving these differences, are not
568 known and require further study.

569 Our results provide evidence of frog skin epithelial cell immunocompetence in
570 establishing a functional antiviral state. Additionally, we observed that prior induction of this
571 antiviral state with poly(I:C) is effective against FV3 immunoevasion mechanisms, thereby
572 highlighting these cells as important contributors to skin innate immune defences. In frog skin,
573 induction of an antiviral state in epithelial cells may require paracrine type I IFN signaling from
574 resident immune cells (e.g. macrophages) or other cell types within the complex skin tissue to

575 initiate an effective anti-FV3 state. Indeed, the restricted tissue necrosis observed in infected
576 frogs supports the eventual establishment of an antiviral state in frog skin tissues. The ability of
577 frog skin epithelial cells to detect and respond to a synthetic viral PAMP analogue suggests that
578 Xela DS2 and Xela VS2 cell lines can be used to identify and/or screen immunomodulatory
579 molecules present in the host or the environment that may impact epithelial cell
580 susceptibility/permissibility to FV3. Thus, in addition to furthering our understanding of antiviral
581 responses of skin epithelial cells to FV3 infection, we believe Xela DS2 and Xela VS2 represent
582 novel *in vitro* platforms for future research in frog epithelial cell-FV3 interactions and
583 immunoevasion mechanisms at the host-environment interface.

584 5. Declaration of Interest

585 The authors declare no conflicts of interest.

586 6. Author contributions

587 **Maxwell P. Bui-Marinós:** conceptualization, methodology, investigation, data curation,
588 formal analysis, writing – original draft, review and editing. **Lauren A. Todd:** data curation,
589 formal analysis, investigation, methodology, visualization, writing - original draft, review and
590 editing. **Marie-Claire D. Wasson:** investigation, writing - review and editing. **Brandon E.E.**
591 **Morningstar:** investigation, formal analysis, writing - review and editing. **Barbara A.**
592 **Katzenback:** conceptualization, methodology, investigation, resources, writing – original draft
593 and review and editing, supervision, funding acquisition.

594 7. Acknowledgements

595 This work was supported by a Natural Sciences and Engineering Research Council
596 (NSERC) Discovery Grant (RGPIN-2017-04218) and University of Waterloo Start-Up Funds to
597 BAK, University of Waterloo Science Graduate Awards to MPB-M, and a NSERC Postdoctoral
598 Fellowship (PDF-546075-2020) to LAT. We thank Dr. Niels C. Bols for providing the FV3
599 strain and EPC cell line used in this study and for kindly permitting us to use their cell culture
600 facilities during the early part of this study, Dr. Nguyen T. K. Vo for providing technical training
601 on FV3 infection procedures and maintenance of the EPC cell line, and Adrienne Ranger for
602 their technical assistance in initial testing of scavenger receptor primers.

603

604 **8. References**

- 605
606 Altschul, S.F., Gish, W., Miller, W., Myers, E.W., Lipman, D.J., 1990. Basic local alignment
607 search tool. *J. Mol. Biol.* 215, 403-410.
- 608 Aranda, P.S., LaJoie, D.M., Jorcyk, C.L., 2012. Bleach gel: a simple agarose gel for analyzing
609 RNA quality. *Electrophoresis* 33, 366-369.
- 610 Ariel, E., Nicolajsen, N., Christophersen, M.-B., Holopainen, R., Tapiovaara, H., Bang Jensen,
611 B., 2009. Propagation and isolation of ranaviruses in cell culture. *Aquaculture* 294, 159-164.
- 612 Bienentreu, J.-F., Grayfer, L., Schock, D.M., Guerreiro, M., Mehes-Smith, M., DeWitte-Orr, S.J.,
613 Robert, J., Brunetti, C.R., Lesbarrères, D., 2020. Sublethal effects of wild-type and a vIF-2 α -
614 knockout Frog virus 3 on postmetamorphic wood frogs (*Rana sylvatica*): potential for a stage-
615 specific reservoir. *FACETS* 5, 737-757.
- 616 Brand, M.D., Hill, R.D., Brenes, R., Chaney, J.C., Wilkes, R.P., Grayfer, L., Miller, D.L., Gray,
617 M.J., 2016. Water temperature affects susceptibility to ranavirus. *Ecohealth* 13, 350-359.
- 618 Braunwald, J., Nonnenmacher, H., Tripier-Darcy, F., 1985. Ultrastructural and biochemical
619 study of frog virus 3 uptake by BHK-21 cells. *J. Gen. Virol.* 66, 283-293.
- 620 Bui-Marinos, M.P., Varga, J.F.A., Vo, N.T.K., Bols, N.C., Katzenback, B.A., 2020. Xela DS2
621 and Xela VS2: Two novel skin epithelial-like cell lines from adult African clawed frog (*Xenopus*
622 *laevis*) and their response to an extracellular viral dsRNA analogue. *Dev. Comp. Immunol.* 112,
623 103759.
- 624 Chinchar, V.G., Bryan, L., Wang, J., Long, S., Chinchar, G.D., 2003. Induction of apoptosis in
625 frog virus 3-infected cells. *Virology* 306, 303-312.
- 626 Dayeh, V.R., Chow, S.L., Schirmer, K., Lynn, D.H., Bols, N.C., 2004. Evaluating the toxicity of
627 Triton X-100 to protozoan, fish, and mammalian cells using fluorescent dyes as indicators of cell
628 viability. *Ecotoxicol. Environ. Saf.* 57, 375-382.
- 629 De Jesús Andino, F., Chen, G., Li, Z., Grayfer, L., Robert, J., 2012. Susceptibility of *Xenopus*
630 *laevis* tadpoles to infection by the ranavirus Frog-Virus 3 correlates with a reduced and delayed
631 innate immune response in comparison with adult frogs. *Virology* 432, 435-443.
- 632 Forzán, M.J., Jones, K.M., Ariel, E., Whittington, R.J., Wood, J., Markham, R.J.F., Daoust, P.-Y.,
633 2017. Pathogenesis of Frog virus 3 (ranavirus, iridoviridae) infection in wood frogs (*Rana*
634 *sylvatica*). *Veterinary Pathology* 54, 531-548.
- 635 Forzán, M.J., Jones, K.M., Vanderstichel, R.V., Wood, J., Kibenge, F.S.B., Kuiken, T., Wirth,
636 W., Ariel, E., Daoust, P.Y., 2015. Clinical signs, pathology and dose-dependent survival of adult
637 wood frogs, *Rana sylvatica*, inoculated orally with frog virus 3 Ranavirus sp., Iridoviridae. *J.*
638 *Gen. Virol.* 96, 1138-1149.
- 639 Fox, H., Whitear, M., 1990. Cellular elements of the dermis and collagen remodelling during
640 larval life of anurans. *Arch. Histol. Cytol.* 53, 381-391.

- 641 Gantress, J., Maniero, G.D., Cohen, N., Robert, J., 2003. Development and characterization of a
642 model system to study amphibian immune responses to iridoviruses. *Virology* 311, 254-262.
- 643 Gendrault, J.L., Steffan, A.M., Bingen, A., Kirn, A., 1981. Penetration and uncoating of frog
644 virus 3 (FV3) in cultured rat Kupffer cells. *Virology* 112, 375-384.
- 645 Grayfer, L., De Jesús Andino, F., Robert, J., 2014. The amphibian (*Xenopus laevis*) type I
646 interferon response to frog virus 3: new insight into ranavirus pathogenicity. *J. Virol.* 88, 5766-
647 5777.
- 648 Grayfer, L., De Jesús Andino, F., Robert, J., 2015a. Prominent amphibian (*Xenopus laevis*)
649 tadpole type III interferon response to the frog virus 3 ranavirus. *J. Virol.* 89, 5072-5082.
- 650 Grayfer, L., Edholm, E., De Jesús Andino, F., Chinchar, V.G., Robert, J., 2015b. Ranavirus host
651 immunity and immune rvasion, in: Gray M., C.V. (Ed.), *Ranaviruses*. Springer, Cham.
- 652 Grayfer, L., Robert, J., 2014. Divergent antiviral roles of amphibian (*Xenopus laevis*)
653 macrophages elicited by colony-stimulating factor-1 and interleukin-34. *J. Leukoc. Biol.* 96,
654 1143-1153.
- 655 Grayfer, L., Robert, J., 2015. Distinct functional roles of amphibian (*Xenopus laevis*) colony-
656 stimulating factor-1- and interleukin-34-derived macrophages. *J. Leukoc. Biol.* 98, 641-649.
- 657 Haislip, N.A., Gray, M.J., Hoverman, J.T., Miller, D.L., 2011. Development and disease: how
658 susceptibility to an emerging pathogen changes through anuran development. *PLoS One* 6,
659 e22307.
- 660 Harp, E.M., Petranka, J.W., 2006. Ranavirus in wood frogs (*Rana sylvatica*): potential sources of
661 transmission within and between ponds. *J. Wildl. Dis.* 42, 307-318.
- 662 Houts, G.E., Gravell, M., Granoff, A., 1974. Electron microscopic observations on early events
663 of frog virus 3 replication. *Virology* 58, 589-594.
- 664 Hoverman, J.T., Gray, M.J., Haislip, N.A., Miller, D.L., 2011. Phylogeny, life history, and
665 ecology contribute to differences in amphibian susceptibility to ranaviruses. *Ecohealth* 8, 301-
666 319.
- 667 Kärber, G., 1931. Beitrag zur kollektiven behandlung pharmakologischer reihenversuche.
668 *Naunyn-Schmiedebergs Arch. Exp. Pathol. Pharmacol.* 162, 480-483.
- 669 Kelly, D.C., 1975. Frog virus 3 replication: electron microscope observations on the sequence of
670 infection in chick embryo fibroblasts. *J. Gen. Virol.* 26, 71-86.
- 671 Knudson, D.L., Tinsley, T.W., 1974. Replication of a nuclear polyhedrosis virus in a continuous
672 cell culture of *Spodoptera frugiperda*: purification, assay of infectivity, and growth
673 characteristics of the virus. *J. Virol.* 14, 934-944.
- 674 Kumar, A., Zhang, J., Yu, F.S., 2006. Toll-like receptor 3 agonist poly(I:C)-induced antiviral
675 response in human corneal epithelial cells. *Immunology* 117, 11-21.
- 676 Lehman, H., 1953. Observations on macrophage behavior in the fin of *Xenopus* larvae. *Biol. Bull.*
677 105, 490-495.

- 678 Lisser, G.J., Vo, N.T.K., DeWitte-Orr, S.J., 2017. Delineating the roles of cellular and innate
679 antiviral immune parameters mediating ranavirus susceptibility using rainbow trout cell lines.
680 *Virus Res* 238, 114-123.
- 681 Miller, D., Gray, M., Storfer, A., 2011. Ecopathology of ranaviruses infecting amphibians.
682 *Viruses* 3, 2351-2373.
- 683 Miller, D.L., Rajeev, S., Gray, M.J., Baldwin, C.A., 2007. Frog virus 3 infection, cultured
684 American bullfrogs. *Emerg. Infect. Dis.* 13, 342-343.
- 685 Petricevich, V.L., Palomares, L.A., Gonzalez, M., Ramirez, O.T., 2001. Parameters that
686 determine virus adsorption kinetics: toward the design of better infection strategies for the insect
687 cell - baculovirus expression system. *Enzyme Microb. Technol.* 29, 52-61.
- 688 Pham, P., Huang, Y., Mosser, D., Bols, N., 2015. Use of cell lines and primary cultures to
689 explore the capacity of rainbow trout to be a host for frog virus 3 (FV3). *In Vitro Cell Dev. Biol.*
690 *Anim.* 51, 894-904.
- 691 Pham, P.H., Jung, J., Bols, N.C., 2011. Using 96-well tissue culture polystyrene plates and a
692 fluorescence plate reader as tools to study the survival and inactivation of viruses on surfaces.
693 *Cytotechnology* 63, 385-397.
- 694 Ritter, M., Mennerich, D., Weith, A., Seither, P., 2005. Characterization of Toll-like receptors in
695 primary lung epithelial cells: strong impact of the TLR3 ligand poly(I:C) on the regulation of
696 Toll-like receptors, adaptor proteins and inflammatory response. *J. Inflamm.* 2, 16.
- 697 Robert, J., Abramowitz, L., Gantress, J., Morales, H.D., 2007. *Xenopus laevis*: a possible vector
698 of Ranavirus infection? *J. Wildl. Dis.* 43, 645-652.
- 699 Robert, J., Edholm, E.S., Jazz, S., Odalys, T.L., Francisco, J.A., 2017. *Xenopus*-FV3 host-
700 pathogen interactions and immune evasion. *Virology* 511, 309-319.
- 701 Robert, J., George, E., De Jesús Andino, F., Chen, G., 2011. Waterborne infectivity of the
702 ranavirus frog virus 3 in *Xenopus laevis*. *Virology* 417, 410-417.
- 703 Rothenburg, S., Chinchar, V.G., Dever, T.E., 2011. Characterization of a ranavirus inhibitor of
704 the antiviral protein kinase PKR. *BMC Microbiol.* 11, 56.
- 705 Varga, J.F.A., Bui-Marinis, M.P., Katzenback, B.A., 2019. Frog skin innate immune defences:
706 sensing and surviving pathogens. *Front. Immunol.* 9, 3128.
- 707 Vo, N.T.K., Guerreiro, M., Yaparla, A., Grayfer, L., DeWitte-Orr, S.J., 2019a. Class A
708 scavenger receptors are used by Frog virus 3 during its cellular entry. *Viruses* 11.
- 709 Vo, N.T.K., Moore, L.C., Leis, E., DeWitte-Orr, S.J., 2019b. Class A scavenger receptors
710 mediate extracellular dsRNA sensing, leading to downstream antiviral gene expression in a novel
711 American toad cell line, BufoTad. *Dev. Comp. Immunol.* 92, 140-149.
- 712 Wendel, E.S., Yaparla, A., Koubourli, D.V., Grayfer, L., 2017. Amphibian (*Xenopus laevis*)
713 tadpoles and adult frogs mount distinct interferon responses to the Frog Virus 3 ranavirus.
714 *Virology* 503, 12-20.

- 715 Wendel, E.S., Yaparla, A., Melnyk, M.L.S., Koubourli, D.V., Grayfer, L., 2018. Amphibian
716 (*Xenopus laevis*) tadpoles and adult frogs differ in their use of expanded repertoires of type I and
717 type III interferon cytokines. *Viruses* 10, 372.
- 718 Winton, J., Batts, W., deKinkelin, P., LeBerre, M., Bremont, M., Fijan, N., 2010. Current
719 lineages of the *epithelioma papulosum cyprini* (EPC) cell line are contaminated with fathead
720 minnow, *Pimephales promelas*, cells. *J. Fish. Dis.* 33, 701-704.
- 721 Yaparla, A., Popovic, M., Grayfer, L., 2018. Differentiation-dependent antiviral capacities of
722 amphibian (*Xenopus laevis*) macrophages. *J. Biol. Chem.* 293, 1736-1744.
- 723

724 **Figure Legends**

725

726 **Figure 1. Xela DS2 and Xela VS2 are susceptible to FV3 and exhibit a loss of cell viability**
727 **at high MOIs.** Xela DS2 and Xela VS2 cells were infected with FV3 by absorption for 2 h at a
728 MOI of 0 (mock-infected), 0.0002, 0.002, 0.02, 0.2, 2 or 20. Over 14 dpi, (A) Xela DS2 and (B)
729 Xela VS2 cell metabolic activity (rezazurin assay) and (C) Xela DS2 and (D) Xela VS2
730 membrane integrity (CFDA-AM assay) were measured on a BioTek Cytation 5 multimode plate
731 reader and imager. Data represent the mean relative fluorescent units \pm standard error and were
732 analyzed with a two-way ANOVA with Tukey's post-hoc test ($p < 0.05$). $n = 4$ independent
733 experiments. Asterisks (*) indicate statistical significance of the infected cells relative to mock-
734 infected cells (MOI 0) within each respective day.

735

736 **Figure 2. Cytopathic effects are observed in FV3-infected Xela DS2 and Xela VS2.**
737 Monolayers of (A) Xela DS2 and (B) Xela VS2 were infected with FV3 by absorption for 2 h at
738 a MOI of 0 (mock-infected), 0.0002, 0.002, 0.02, 0.2, 2 or 20 and cell morphology was
739 documented over 7 dpi. Phase contrast images were captured at 200 \times magnification using a
740 Leica DMi1 microscope (scale bar is 100 μ M). The images shown are representative of four
741 independent trials.

742

743 **Figure 3. Xela DS2 and Xela VS2 are permissive to FV3.** Monolayers of (A) Xela DS2
744 (passage 129 – 139) and (B) Xela VS2 (passage 134 – 139) were infected with FV3 by
745 absorption for 2 h at a MOI of 0 (mock-infected), 0.0002, 0.002, 0.02, 0.2, 2 or 20. Monolayers
746 were washed three times with APBS to remove non-absorbed virus, and low serum media was
747 added to the monolayers. Virus-containing media was removed 30 min after addition (day 0) and
748 at 1, 3, 5 and 7 dpi. Samples were serially diluted and applied to EPC monolayers and wells were
749 scored for CPE after 7 dpi to determine TCID₅₀/mL values. CPE were not observed in EPC
750 monolayers treated with cell culture media collected from mock-infected (A) Xela DS2 or (B)
751 Xela VS2 at any time point. Data were log₁₀ transformed and are presented as the mean \pm
752 standard error of four independent experiments.

753

754 **Figure 4. Transcripts corresponding to known *X. laevis* class A scavenger receptors are**
755 **virtually undetectable in Xela DS2 and Xela VS2.** Total RNA was isolated from Xela DS2
756 (passages 28, 29 and 31) and Xela VS2 (passages (42, 46 and 48), as well as control tissues
757 (spleen, dorsal skin and ventral skin). RT-PCR targets included *X. laevis* *srai/ii*, *scara3*, *scara4*,
758 *scara5* and *marco* transcripts. Amplification of *actb* served as an endogenous control, while
759 amplification of *actb* in cDNA samples prepared without reverse-transcriptase (-RT) indicated
760 the absence of contaminating genomic DNA.

761
762 **Figure 5. Xela DS2 and Xela VS2 do not upregulate antiviral transcripts following**
763 **challenge with UV-inactivated FV3 or FV3.** Xela DS2 or Xela VS2 were mock-infected
764 (media), treated with 1 $\mu\text{g}/\text{mL}$ poly I:C (pIC), challenged with UV-inactivated FV3 at a MOI of
765 2 or infected with FV3 at a MOI of 2 for 6 h, 24 h, 48 h or 72h. RT-qPCR was performed using
766 cDNA generated from each treatment and time point to determine relative transcript levels of
767 (A,B) *ifn*, (C,D) *mx2*, and (E,F) *pkr*. The type I IFN primer set (*ifn*) targets a highly conserved
768 region of *X. laevis* *ifn3*, *ifn4*, *ifn6* and *ifn7*. Data were analyzed using the $\Delta\Delta\text{Ct}$ method and were
769 expressed as a fold-change in transcript levels relative to that of the 6 h non-treated control
770 sample. Data represent the mean \pm standard error and were analyzed with a Kruskal-Wallis test
771 and Dunn's post-hoc test. $n = 4$ independent experiments. Within each time point, significant
772 statistical differences ($p < 0.05$) are denoted using a lettering system, wherein groups with the
773 same lettering are not statistically different.

774
775 **Figure 6. Xela DS2 and Xela VS2 do not upregulate proinflammatory gene transcripts**
776 **following challenge with UV-inactivated FV3 or FV3.** Xela DS2 or Xela VS2 were mock-
777 infected (media), treated with 1 $\mu\text{g}/\text{mL}$ poly I:C (pIC), challenged with UV-inactivated FV3 at a
778 MOI of 2 or infected with FV3 at a MOI of 2 for 6 h, 24 h, 48 h or 72h. RT-qPCR was
779 performed using cDNA generated from each treatment and time point to determine relative
780 transcript levels of (A,B) *il1b*, (C,D) *tnf*, (E,F) *cxcl8a*, and (G,H) *ikb*. Data were analyzed using
781 the $\Delta\Delta\text{Ct}$ method and were expressed as a fold-change in transcript levels relative to that of the 6
782 h non-treated control sample. Data represent the mean \pm standard error and were analyzed with a
783 Kruskal-Wallis test and Dunn's post-hoc test. $n = 4$ independent experiments. Within each time

784 point, significant statistical differences ($p < 0.05$) are denoted using a lettering system, wherein
785 groups with the same lettering are not statistically different.

786

787 **Figure 7. High concentrations of poly(I:C) are cytotoxic to Xela DS2 and Xela VS2.** Xela
788 DS2 and Xela VS2 were treated with 0, 10, 50, 100, 1,000 or 10,000 ng/mL poly(I:C) for 1, 2, 3
789 and 5 days. Cell metabolic activity for (A) Xela DS2 and (B) Xela VS2 was assessed using a
790 resazurin assay and cell membrane integrity for (C) Xela DS2 and (D) Xela VS2 was assessed
791 with CFDA-AM assay. Data are expressed as percent change in fluorescence intensity relative to
792 that of 0 ng/mL poly(I:C) control group at day 1 post-treatment for each cell line and assay. Data
793 represent the mean \pm standard error. $n = 3$ independent experiments. Data were analyzed with a
794 two-way ANOVA and Tukey's post-hoc test. Within each time point, significant statistical
795 differences ($p < 0.05$) are denoted using a lettering system, wherein groups with the same
796 lettering are not statistically different.

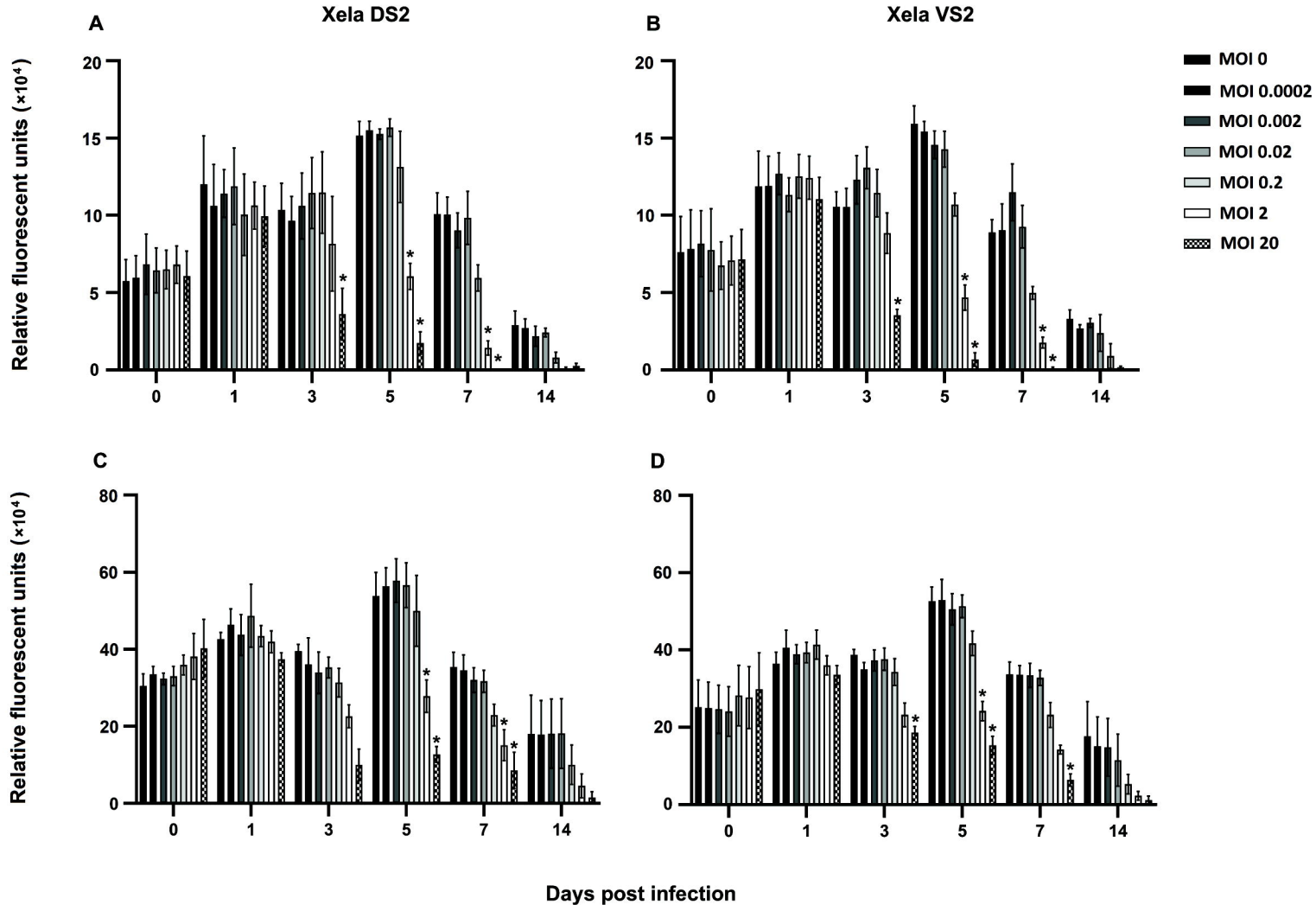
797

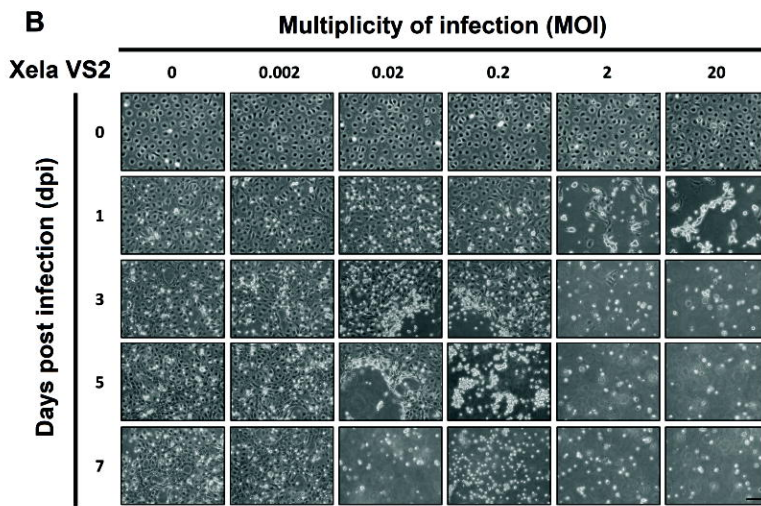
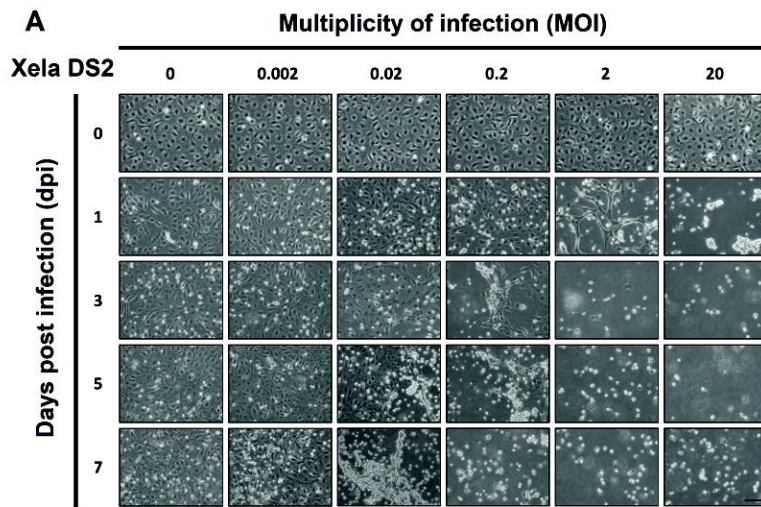
798 **Figure 8. Pretreatment of Xela DS2 and Xela VS2 with poly(I:C) mitigates FV3-induced**
799 **loss of cell adherence.** Xela DS2 and Xela VS2 were pre-treated with 0, 10, 50, or 100 ng/mL
800 poly(I:C) for 24 h before mock-infection or FV3 infection (MOI 2) of cells by absorption for 2 h.
801 On 0, 3, and 5 dpi, cell culture media was removed and the number of adherent (A) Xela DS2
802 and (B) Xela VS2 cells was determined by enumerating NucBlue Live-stained nuclei using the
803 fluorescent imaging and cell count feature of the BioTek Cytation 5 Gen5 software. Cell viability
804 of adherent (C) Xela DS2 and (D) Xela VS2 was assessed using the metabolic-based resazurin
805 assay. Data represent the mean \pm standard error. $n = 3$ independent experiments. Data were
806 analyzed with a two-way ANOVA and Tukey's post-hoc test. Significant statistical differences
807 ($p < 0.05$) across all groups are denoted using a lettering system, wherein groups with the same
808 lettering are not statistically different.

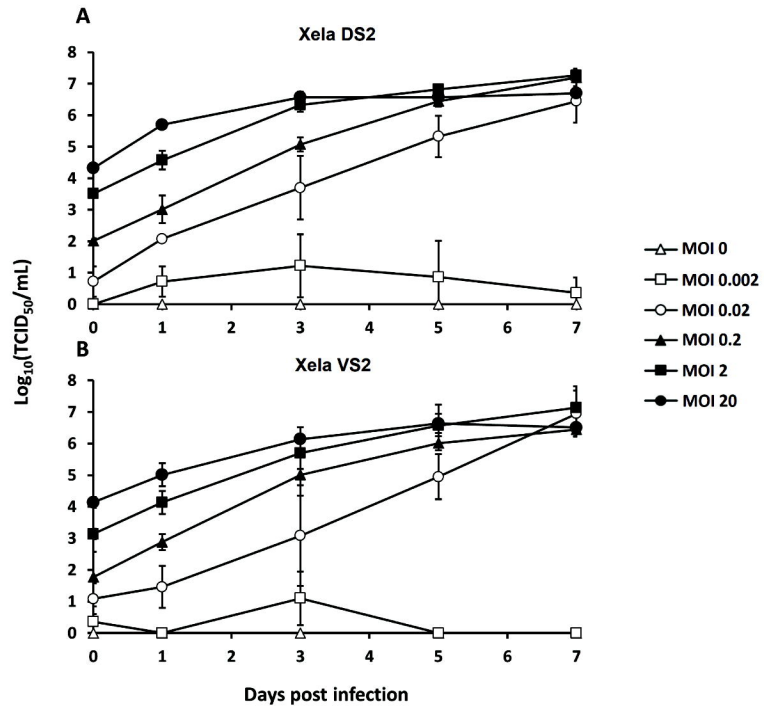
809

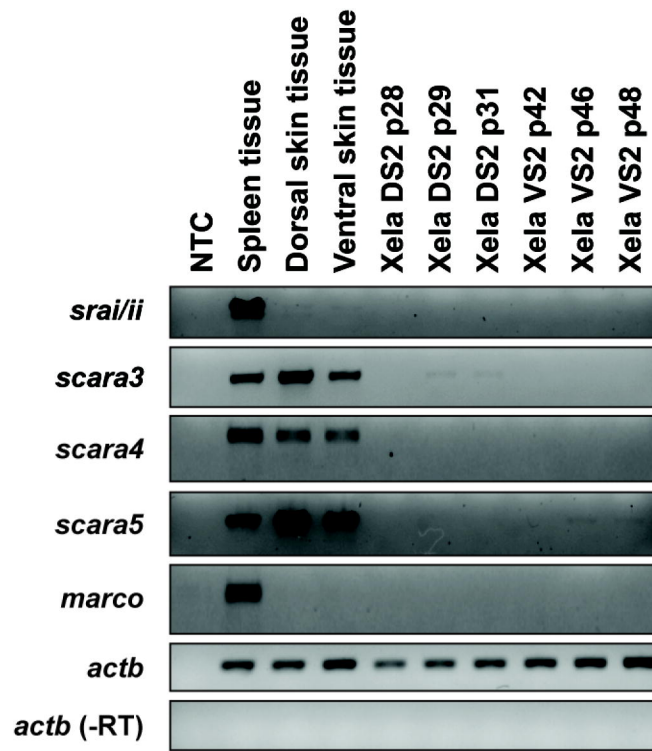
810 **Figure 9. Poly(I:C) pretreatment limits FV3 replication in Xela DS2 and Xela VS2.** Xela
811 DS2 and Xela DS2 were pre-treated with 0 or 100 ng/mL poly(I:C) for 24 h before FV3 infection
812 (MOI 2) of cells by absorption for 2 h. Following pretreatment and infection, virus-containing
813 media was collected from (A) Xela DS2 and (B) Xela VS2 at 0, 3, and 5 dpi and used to
814 determine TCID₅₀/mL values. Data were log₁₀ transformed and are presented as the mean \pm

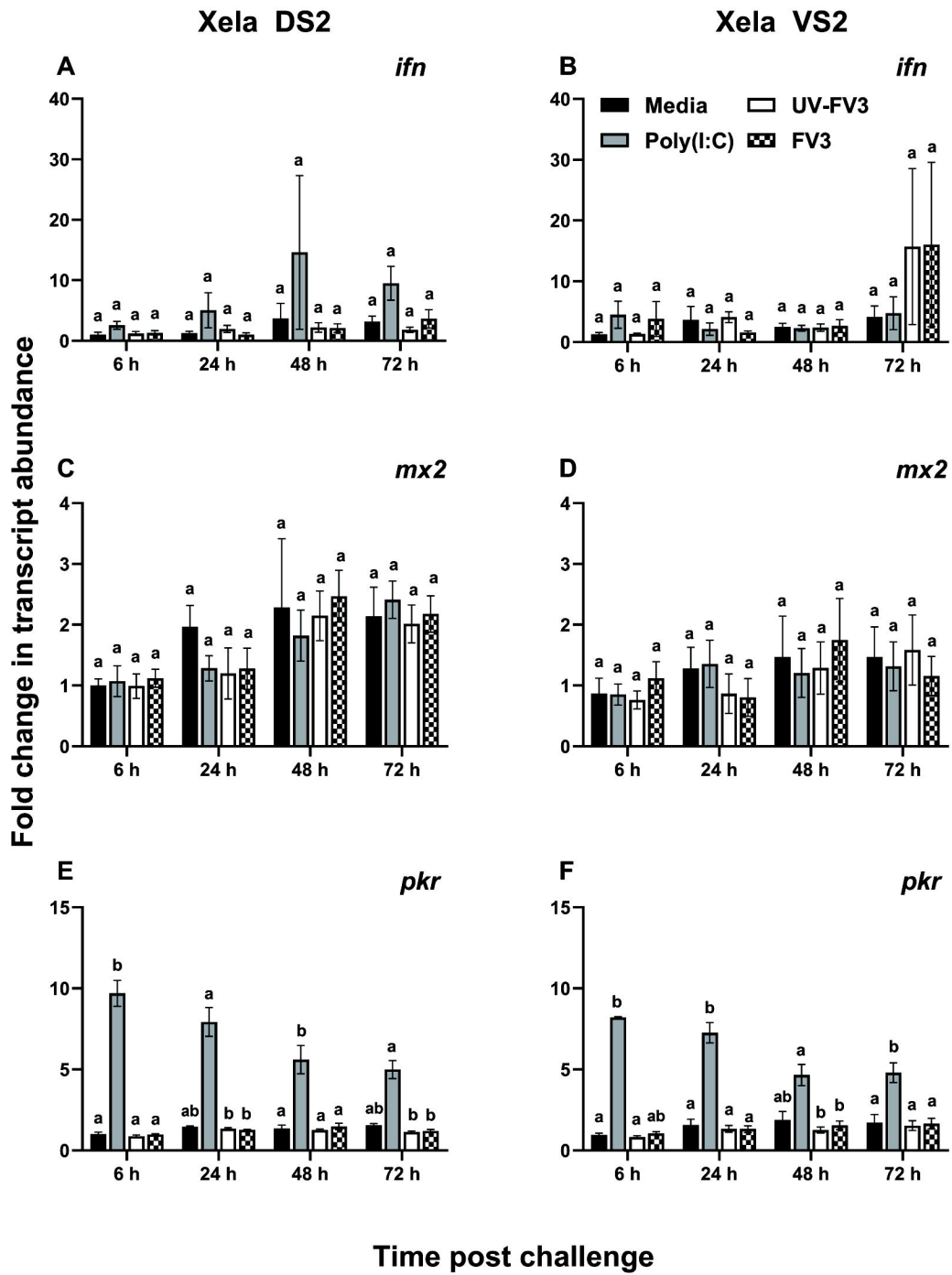
815 standard error of three independent experiments. Data were analyzed with a two-way ANOVA
816 and Tukey's post-hoc test. Significant statistical differences ($p < 0.05$) are denoted using a
817 lettering system, wherein groups with the same lettering are not statistically different.

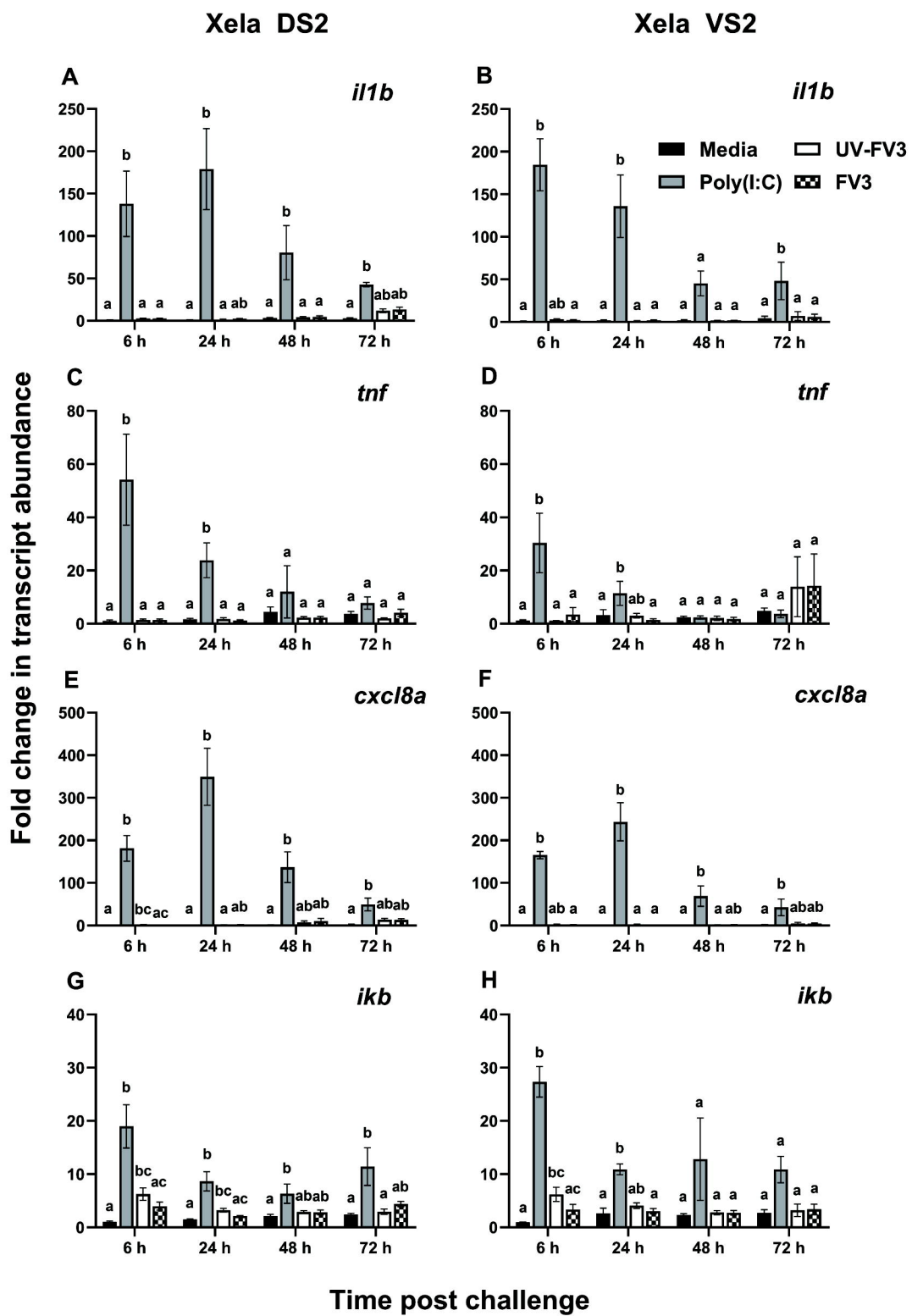


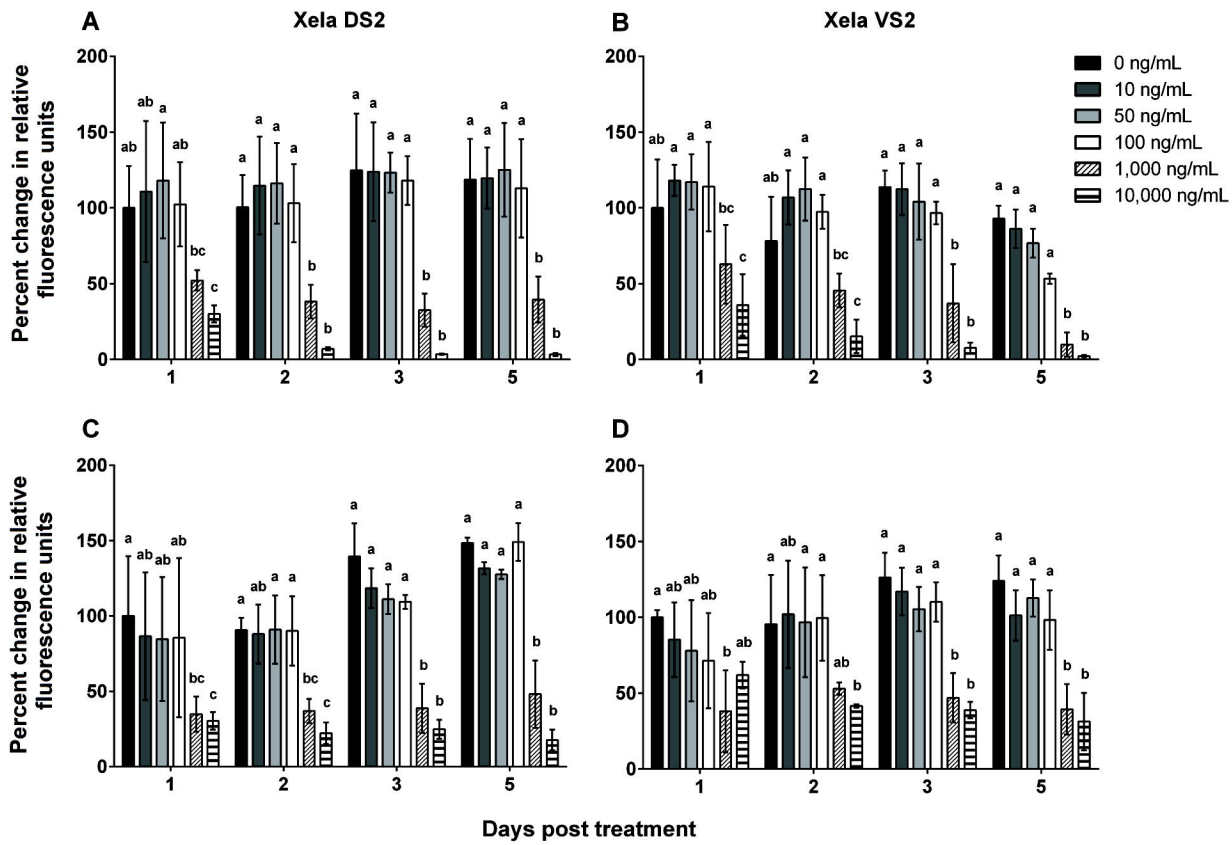












Days post treatment

